Applied Geochemistry 158 (2023) 105806

Contents lists available at ScienceDirect

Applied Geochemistry

journal homepage: www.elsevier.com/locate/apgeochem

Antimony and arsenic behaviour in lead/zinc mine tailings during storage under vegetation cover

I.T. Burke [a,*], R. Courtney [b], W.M. Mayes [c]

[a] School of Earth and Environment, University of Leeds, Leeds, LS2 9JT, UK
[b] Department of Biological Sciences, University of Limerick, Limerick, V94 T9PX, Ireland
[c] School of Environmental Sciences, University of Hull, Hull, HU6 7RX, UK

ARTICLE INFO

Editorial handling by Mahyar Yousefi

Keywords:
Arsenic
Antimony
XANES
Mine tailings
Oxidation
Revegetation

ABSTRACT

The high-volume, fine grained tailings produced from Pb/Zn ore processing need to be carefully managed. Metalloid elements, As and Sb, are present in tailings at ~800 and ~80 mg kg^{-1} respectively, and in neutral pH leachates at 5–50 μg L^{-1}. Despite these relatively low leachate concentrations, As and Sb can cause regulatory concern due to their high toxicity and propensity for bioaccumulation. As and Sb mobility in tailings are controlled by their chemical speciation and associations with mineral phases. Changes in As and Sb speciation were, therefore, determined in depth profile samples taken from an active tailings management facility during waste storage up to 8 years since deposition. At this site, primarily to prevent dust formation, a vegetation cover was established by addition of organic compost to surface layers and seeding grasses. Over time a robust vegetation cover was established consisting of perennial grasses, clovers, and after 8 years, small trees and shrubs. The surface layer of the tailings also became progressively more oxidised over time producing a substrate more suitable for plant growth enabling the establishment of beneficial vegetation cover and the development of a thin soil-like surface layer. As and Sb were both present in predominately reduced 3+ forms in freshly deposited tailings but were converted to oxidised 5+ forms in older samples. Oxidation of Fe(II) in pyrite also occurred, producing increased amounts of weak acid leachable Fe(III)-oxides in the tailings. Sorption of As to neoformed iron oxides in leachate drains reduced concentrations in leachates to below regulatory limits, but Sb sorption was relatively ineffective resulting in higher Sb concentration in site drainage waters, which may require specific treatments to reduce Sb concentrations prior to discharge.

1. Introduction

Mine tailings are the high-volume waste produced after separation of the valuable components of ores from minerals of no economic value. Management of mine tailings is a globally significant issue due to concerns over safe disposal of solids and aqueous leachates (Kossoff et al., 2014). Carbonate-hosted lead-zinc deposits are the primary source for these two metals and are mined in every continent except Antarctica. Typically, they contain hydrothermal Pb- and Zn- sulphide ores (galena, PbS; sphalerite, ZnS) hosted in carbonate rocks such as limestone or dolomite (Guilbert and Park jr, 2007). Tailings produced from such ores are often low in sulphide content relative to neutralising carbonate phases, thus typically produce neutral (pH 6–9) drainage waters (Othmani et al., 2013; Li et al., 2022a). Although neutral mine drainage is typically less environmentally damaging than leachates from acid generating mine wastes, aqueous metal(loid) concentrations can still be of concern and may be the most prevalent mine pollution pressures in some jurisdictions, and require suitable management (Jones et al., 2013).

Processing of lead-zinc ores involves the separation of the Pb- and Zn- sulphide minerals from other minerals present, such as carbonate and silicate minerals. During ore processing, tailings are typically produced in amounts that greatly exceed the products and are disposed of at the site of production (Mudd and Boger, 2013), and often requiring a purpose-built tailings management facility (TMF). The separation of metalliferous components is never perfect, and the tailings often contain contaminant metal(loids) including Pb, Zn, As and Sb at 100–1000 s mg kg^{-1} concentrations (Othmani et al., 2013). During initial processing the ores are milled to grainsizes <200 μm (Su et al., 2019; Romero et al., 2007), which promotes leaching when the tailings become saturated

* Corresponding author.
E-mail address: i.t.burke@leeds.ac.uk (I.T. Burke).

https://doi.org/10.1016/j.apgeochem.2023.105806
Received 6 July 2023; Received in revised form 18 September 2023; Accepted 7 October 2023
Available online 10 October 2023

with water during disposal. Lead-zinc tailings leachates are often pH neutral (pH 6–9) and can contain Pb and Zn at mg L^{-1} concentrations (Fitzsimons and Courtney, 2022; Hudson-Edwards et al., 2003). In addition, the presence of μg L^{-1} amounts of trace elements (such as As and Sb) in leachates can cause regulatory concern due to their high aquatic toxicity and potential for uptake into plants (Heikkinen et al., 2009; Plante et al., 2011; Olszewska et al., 2016; Hudson-Edwards et al., 2019; Warnken et al., 2017).

It is often desirable to establish a vegetation cover on tailings during disposal, primarily for dust suppression and stability. However, there are relatively few studies of the effect of vegetation on contaminant behaviour (Jordan et al., 2008; Chambers and Sidle, 1991) and previous work has not specifically focused on the mobility of metal(loid) elements that occur at lower concentrations in tailings, such as As and Sb. Previous work has shown that vegetation growth on wastes can alter the substrates, forming a soil-like layer and making them more amenable for plant and bacterial colonisation (Bray et al., 2018). As and Sb are expected to be primarily present in the lead/zinc ores in a range of sulphide-associated As(III) and Sb(III) phases (Yesares et al., 2022; Wilkinson et al., 2005; Janković et al., 1977). However, ore processing will increase reactive surface area and expose tailings to oxygenated water, which may lead to rapid oxidation of any remnant sulphide phases carried over to the tailings. Sulphide oxidation is expected to promote the formation As(III/V) and Sb(III/V) oxyanion species (Rickard, 2012) that may be solubilised into tailings porewaters and leachates. Such oxyanions are also susceptible to redox transformations (e.g. after burial below vegetation cover) that may also affect their leaching potential. At neutral pH, As and Sb oxyanions can have contrasting environmental behaviour. As(III)-species generally sorb less strongly to solids and are therefore more mobile than As(V)-species (Raven et al., 1998; Johnston et al., 2020a) but the opposite is observed for Sb(III) and Sb(V) species (Guo et al., 2014). Therefore, redox processes that favour retardation of one of these metalloids may promote increased mobility of the other. Therefore, it is important to understand how trace contaminant speciation changes during processing and tailings storage to accurately predict long term leaching behaviour and inform future waste management decisions.

At the Tara Boliden Mine (the largest active zinc mine in Europe) lead-zinc ore concentrates from a carbonate-hosted deposit are milled to ~150 μm and the valuable Pb- and Zn- sulphide minerals are separated from host rocks. The tailings waste produced is predominated by carbonate and silicate minerals and is disposed of as backfill within mine tunnels and in tailings impoundments capped with vegetation cover (Fitzsimons and Courtney, 2022). Previous observations (2019–2021) of leachate present at this site recorded mean As concentrations of 6 μg L^{-1} (range, 5–10 μg L^{-1}) and mean Sb concentrations of 18 μg L^{-1} (range, 7–46 μg L^{-1}) in perimeter drain samples (Fitzsimons and Courtney, 2022), compared with EU regulatory drinking water limits for As of 10 μg L^{-1} and Sb of 5 μg L^{-1} (McGrory et al., 2017; Filella et al., 2002). This was despite As being more concentrated in the tailings than Sb (620 mg kg^{-1} versus 80 mg kg^{-1}; (Fitzsimons and Courtney, 2022)). Furthermore, plant growth trials using similar tailings as the growth substrate have shown elevated As and Sb in root and shoot samples (Proto et al., 2022), which indicates that these metalloids can become mobilised in pore solutions.

The mechanism and phases controlling these metalloid releases are currently unknown. The aim of this paper is to use X-ray Absorption near edge structure (XANES) analysis to determine As and Sb speciation in mine tailings recovered from an active lead zinc mine TMF. We have collected samples over time after deposition in the tailings impoundment to investigate how processing and tailing storage affects metalloid speciation. Also, water and solid samples from the perimeter wall drainage are examined to determine if processes occurring when leachate emerges from the tailings can control metalloid transport into receiving waters. This new information will be integrated to allow better prediction of how the hazards associated with As and Sb leaching from tailings are affected by the environmental conditions during disposal; and allowing for better environmental regulation and informing waste management practices at both legacy and active mine sites.

2. Materials and methods

Mine Tailings Samples: Tailings materials were recovered in April 2022 from the tailings management facility (TMF) at the Boliden Tara Mine, Ireland (SI Fig. S1). At this TMF, vegetation cover was established on freshly deposited tailings to stabilise the tailings surface and aid in dust suppression. After deposition, tailings were seeded with perennial grasses and surface amended with organic matter (spent mushroom compost). Tailings samples collected included: 1) A sample of freshly produced mine tailings (sample code: 0Y); 2) a 0–5 cm near surface sample from an unseeded 1 year old tailings impoundment (1Y); 3) a 25 cm core recovered using a 5 cm diameter hand auger from a seeded 3 year old tailings impoundment (3Y); and 4) a 25 cm core of 8 year old seeded tailings (8Y) recovered from a 1 m^3 free draining outdoor bulk container (located adjacent to the TMF). Tailings samples were placed into polypropylene containers prior to being transported to the University of Leeds, where they were refrigerated (4 °C) prior to processing. During processing, subsamples from the cores were taken from a 2–3 cm surface layer (just below rootlet level), and subsequently at 5 cm intervals below this layer. To help stabilise these potentially air sensitive samples, all subsamples were dried under a 97% N_2: 3% H_2 atmosphere in an anaerobic chamber (Coy Ltd., USA) at room temperature (18 ± 3 °C) and gently disaggregated and homogenised using a porcelain mortar and pestle prior to use in subsequent analysis. Colour was ascribed to dried samples using Munsell soil colour charts.

Drainage samples: Surface water samples were collected in September 2022 after a prolonged period of relatively low precipitation. Drainage at the site is radial from the TMF via a number of perimeter wall drains, which are combined into a single circular perimeter drain. Leachates are either treated, used during ore processing or recirculated back onto the TMF (Fitzsimons and Courtney, 2022). Water samples were collected from two locations within one of the TMF perimeter wall drains receiving leachate from the tailings (at an upper location near to the point of emergence and a lower location near to the point of discharge into the perimeter drain; SI Fig. S2). Water was also collected from the TMF perimeter drain downstream from the point of mixing with the wall drain. Water pH, conductivity and ORP were determined in the field using a Myron Ultrameter 6Psi (field ORP values were converted to Eh versus the standard hydrogen electrode by addition of 199 mV). A solid sample of reddish yellow (Munsell 2.5 YR 7/8) ochre precipitate (PPT) was also recovered from the wall drain. All water samples were filtered (0.2 μm, PES) and acidified by addition of HNO_3 (AR grade, final pH = <2) prior to analysis by ICP-OES/MS (ThermoFisher iCAP 7400 Radial ICP-OES for Zn and S and ThermoFisher iCAP Qc ICP-MS for all other elements). Major anions (SO_4^{2-}, Cl^-) and cations (Ca^{2+}, Mg^{2+}, Na^+, K^+) were determined in the site drainage waters by ion chromatography using a ThermoScientific ICS5000.

Water soluble metalloids: Water extractable As and Sb were determined after 5 ± 0.05 g samples of dried tailings material were mixed with 10 mL of ultrapure water (18.5 MΩ) and shaken at room temperature for 7 days (Bray et al., 2018). The solution pH was measured using an Orion DualStar pH/ISE benchtop meter and electrodes calibrated at pH 4, 7, and 10. Supernatant solutions from the water extractions were filtered (0.2 μm; PES) and acidified with HNO_3 for subsequent analysis by ICP-OES/MS. Extractable Fe(II) and Fe(total) in solids were determined using UV–vis spectroscopy after extractions of 0.1 ± 0.01 g dried samples in 5 mL 0.5 N HCl and reaction of the filtered (0.2 μm; PES) supernatant with Ferrozine (Lovley and Phillips, 1986).

Tailings composition: Major and minor element analysis of selected tailings samples and the drain precipitate were determined using a PANalytical Axios sequential X-ray fluorescence spectrometer (loss on ignition was determined at 1050 °C). Mineralogical analysis was

performed using 50 − 100 mg powder samples mounted on silicon slides on a Bruker D8 X-ray diffractometer (XRD) using Cu Kα radiation and scanning between 2° and 70° 2θ. Relative phase abundance was assigned as follows: Major, Principal (100) Bragg reflection peak height was 51–100% of the largest peak present in the diffractogram; minor, principal peak height was 10–50% of largest peak; trace, principal peak height <10% of the largest peak.

X-Ray Absorption Spectroscopy (XAS): Antimony and arsenic K-edge XAS spectra were collected at beamline B18 of the Diamond Light Source synchrotron, UK in May 2022. Mine tailings samples were prepared as 8 mm diameter (150–200 mg) pressed powder pellets held in Kapton™ tape. The use of dried pelletized samples increased As and Sb concentrations in the cross-sectional beam area in order to improve the signal to noise ratios in the resultant XAS spectra. The Sb K-edge at 30.5 keV was scanned using a Si(311) monochromator in fluorescence mode using a Silicon 32 element X-ray fluorescence detector, and X-ray absorption spectra were collected (k = 0–12 $Å^{-1}$) using a liquid nitrogen cryostat (76–80 K). As K-edge (11.9 keV) XAS spectra (k = 0–12 $Å^{-1}$) were collected using a Si(111) monochromator at room temperature (296–298 K). On beamline B18, the X-ray beam at the sample was 1 mm^2 and no changes in Sb and As XANES spectra were observed between subsequent scans due to beam damage. XAS spectra was also be collected from a range of standard materials (prepared as pressed pellets diluted with cellulose) to allow comparison with sample spectra and linear combination fitting of sample data. Representative standards were selected that contained similar atomic bonding environments present in the samples. These included: stibnite (Sb_2S_3), arsenopyrite (FeAsS), Sb_2O_3, As_2O_3, Sb_2O_5, and $Ca_3(AsO_4)_3$. Sb and As spectra were calibrated for drift in E_0 position using Sb(0)- and Ag(0)- foils respectively. The relevant reference foil spectra were collected in line with samples and standards and were available separately for each spectra. An additional Sb(V) adsorbed to ferrihydrite (Sb(V)-FH) XANES spectra was provided from published data (Johnston et al., 2020a) collected at the 1.9T Wiggler XAS Beamline of the Australian Synchrotron. Access to Athena data (including Sb(0)-foil calibration data) was provided by the authors allowing a precise energy calibration between the Sb(V)-FH standard and the data collected in this study.

For both Sb and As, multiple 3 min XAS scans were summed (to improve data quality), background subtracted in Athena (Ravel and Newville, 2005), and normalised XANES data were plotted. Fourier transformations (FT) of Extended X-ray Absorption Fine Edge Structure (EXAFS) data were also plotted and examined to determine the nature of the Sb(III) bonding environment. In FT plots, with no adjustment for phase shifting, Sb(III)–S bonds produce a FT peak at ~2.0 Å and Sb(III)–O bonds produce FT peak at ~1.5 Å (Bennett et al., 2017). A similar separation in As–S (~2.0 Å) and (~1.4 Å) As–O bonding can also be observed. Linear combination fitting (LCF) was used (also in Athena) to estimate the percentage contribution of selected end member spectra to sample spectra. End member spectra were chosen to best represent the sample spectra (see results section below). Antimony LCF analysis used the $Sb_2(III)O_3$ and Sb(V)-FH standards to fit 1st derivative Sb K-edge XANES data. Arsenic LCF analysis used the FeAs(III)S and $Ca_3(As(V)O_4)_2$ standards to fit As K-edge XANES data. LCF was forced by the software to produce outputs that summed to 100% and uncertainty values were typically ±3%.

3. Results

3.1. Sampling observations

The 1 year old sample was taken from an unvegetated part of the TMF, however adjacent seeded plots had a sparse grass cover (SI Fig. S3). The 3 year old plots had a more diverse vegetation cover consisting of perennial grasses and trifoliate clovers (e.g. *Trifolium repens*). The 8 year old lysimeters had a similar diverse vegetation cover which also included self-seeded shrubs (*Salix* spp.). The 1 year old tailings had no rootlet zone. Rootlets were concentrated to the upper few centimetres in the 3 year tailings, although occasional deeper roots were observed. The 8 year old tailings had roots throughout the depth sampled. The fine grained, fresh dried tailings material was grey (Munsell N 6/1; SI Table S1) and the surface samples recovered from 1 year old tailings was light grey (Munsell N 7/1). In the 3 year old tailings, there was a distinct colour change observed between the core top sample (pale brown, Munsell 2.5Y 8/2) and deeper samples that were grey and light grey in colour. The samples of 8 year old tailings were all uniformly pale brown in colour.

3.2. TMF drainage composition

The water in the upper wall drain had a conductivity of 3530 µS cm^{-1} and pH of 7.9 (Table 1). Conductivity was progressively lower in the lower wall drain and perimeter drain (2490 and 1500 µS cm^{-1} respectively), and pH increased from 8.0 to 8.5. Eh also increased between the upper and lower wall drains and the perimeter drain (184, 236, 309 mV respectively). Aqueous sulphate concentrations decreased by a factor of 2.5 from 1200 mg L^{-1} to 488 mg L^{-1} between the upper wall drain and perimeter wall drain, a similar ratio in values was observed for conductivity. Other cations and anions (Ca^{2+}, Mg^{2+}, K^+, Na^+, Cl^-) also decreased in concentration between 1.6 and 3.0 times between the upper wall and perimeter drains. Metal(loid) concentrations decreased by greater amounts relative to sulphate (especially Fe and Mn, >40 fold reductions) with the exception of Sb that very slightly increased in concentration downstream (Table 1).

3.3. Bulk tailings composition

The tailings material was primarily composed of carbonate minerals (calcite, dolomite), silicates (quartz, feldspar, mica) and trace amounts of pyrite (Table 2; SI Fig. S4). Gypsum was also detected in samples aged for more than 1 year in the TMF. The mineralogy reflected the elemental analysis, with samples dominated by SiO_2 (19–39 wt%) and CaO (24–35 wt%), with minor amounts of Al_2O_3, TiO_2, K_2O, Fe_2O_3 and SO_3 (Table 3). Metal(loid) concentrations were relatively consistent between all samples, which contained; 3450 ± 700 mg kg^{-1} Pb, 3000 ± 970 mg kg^{-1} Zn, 800 ± 230 mg kg^{-1} As and, 80 ± 20 mg kg^{-1} Sb, with no apparent trends in bulk composition with either sample age or depth (Table 3).

The wall drain ochre precipitate was composed primarily of ferrihydrite with trace amounts of calcite, quartz and gypsum (Table 2). Its elemental composition (Table 3) was dominated by Fe_2O_3 (53 wt%) with significant amounts of SiO_2 (9 wt%) and CaO (6 wt%) also present. The

Table 1
Water composition and selected metal(loid) concentrations in TMF drain waters.

Location	Upper Wall Drain	Lower Wall Drain	Perimeter Drain	UWD/PD*
pH	7.9	8.0	8.5	–
Conductivity (µS cm^{-1})	3530	2490	1500	2.3
Eh (mV)	184	236	309	–
Ca (mg L^{-1})	400	n.d.	224	1.6
K (mg L^{-1})	26.7	n.d.	10.2	2.6
Mg (mg L^{-1})	87	n.d.	46	1.9
Na (mg L^{-1})	116	n.d.	38	3.0
SO_4 (mg L^{-1})	1200	n.d.	488	2.5
Cl (mg L^{-1})	80	n.d.	51	1.6
Fe (µg L^{-1})	4080	n.d.	88	46
Mn (µg L^{-1})	542	n.d.	13	43
As (µg L^{-1})	86	n.d.	8.0	11
Pb (µg L^{-1})	2.8	n.d.	0.5	5.4
Sb (µg L^{-1})	1.4	n.d.	1.8	0.8
Zn (µg L^{-1})	2850	n.d.	165	17

n.d. = not determined; *Ratio of values in the upper wall drain to perimeter drain.

Table 2
Tailings and wall drain precipitate (PPT) mineral composition.

Age (yr)	Depth (cm)	Calcite ($CaCO_3$)	Quartz (SiO_2)	Dolomite $CaMg(CO_3)_2$	Albite ($NaAlSi_3O_8$)	Microcline ($KAlSi_3O_8$)	Muscovite ($KAl_2Si_3AlO_{10}(OH)_2$)	Pyrite (FeS_2)	Gypsum ($CaSO_4.2H_2O$)	Ferrihydrite ($Fe_{10}O_{14}(OH)_2$)
0	n.a.	+++	++	++	+	+	+	+	–	–
0	PPT	+	+	–	–	–	–	–	+	+++
1	0–5	+++	++	++	++	+	+	+	–	–
3	0	+++	++	++	+	+	+	+	+	–
3	10	+++	++	++	+	+	+	+	+	–
3	20	+++	++	++	+	+	+	+	+	–
8	0	+++	++	++	+	+	+	+	+	–
8	10	+++	++	++	+	+	+	+	+	–
8	20	+++	++	++	+	+	+	+	+	–

+++ Major phase; ++ Minor phase; + Trace; – not detected; n.a. not applicable.

Table 3
Elemental composition of fresh and aged lead-zinc mine tailings and the wall drain precipitate (PPT).

Element	Age (yr) Depth (cm)	0 n.a.	0 PPT	1 0-5	3 0	3 10	3 20	8 0	8 10	8 20
Major elements (nominal oxides, wt%)										
MgO		3.0	0.4	2.0	3.1	1.9	3.4	2.3	2.6	2.9
Al_2O_3		4.7	0.5	4.0	4.3	4.2	4.0	4.6	4.3	4.6
SiO_2		24.2	8.8	38.7	18.8	19.4	19.9	20.4	19.3	20.8
SO_3		3.6	0.7	3.9	5.4	5.4	7.9	5.3	6.3	6.4
P_2O_5		0.1	0.1	0.1	0.2	0.1	0.1	0.1	0.2	0.2
K_2O		1.6	0.1	1.8	1.4	1.5	1.5	1.5	1.5	1.6
CaO		30.6	5.6	23.6	30.6	34.6	31.3	31.4	32.3	30.6
TiO_2		0.2	0.03	0.2	0.2	0.2	0.2	0.2	0.2	0.2
MnO		0.2	1.2	0.1	0.2	0.2	0.2	0.1	0.2	0.2
Fe_2O_3		2.8	52.8	2.2	3.7	2.6	3.9	3.3	3.3	3.2
LOI @1050 °C		*25.2*	*16.6*	*19.1*	*28.4*	*26.5*	*23.9*	*26.0*	*26.0*	*25.0*
TOTAL		96.6	87.2	96.3	96.7	97.0	96.7	95.6	96.3	96.0
Minor Elements (mg kg^{-1})										
Ba		20921	125	15419	25236	23561	26605	30355	27580	29119
V		31	10	12	35	28	29	30	31	32
Cr		131	11	49	160	174	160	106	101	88
Ni		69	360	49	108	76	88	95	79	79
Cu		117	n.d.	26	156	134	123	154	145	143
As		686	8883	435	957	593	931	1177	868	780
Sr		1513	1154	1098	1659	1822	1600	2275	2235	2190
Sn		43	n.d.	49	53	52	65	59	56	42
Sb		72	24	48	76	77	66	111	90	79
W		12	n.d.	141	19	10	15	12	14	14
Zn		2383	112066	2964	4724	2891	3437	3701	3836	3565
Pb		3225	60	875	3487	3023	2768	4239	3393	2952

sample was also enriched in Zn (11.2 wt%) and some other elements (As, 8880 mg kg^{-1}; Ni, 360 mg kg^{-1}) compared to the tailings compositions. However, other elements, such as Pb and Sb, had lower concentration in the precipitate (60 and 24 mg kg^{-1} respectively) than in the tailings (Table 3).

3.4. Antimony K-edge XANES

Peaks present in Sb K-edge first derivative XANES spectra collected from tailings samples (Fig. 1) demonstrate a mix of both Sb(III) and Sb (V) phases are present. Examination of Fourier transformed Sb K-edge EXAFS data (SI Fig. S5; not phase shifted) show that all samples have peaks at ~1.5 Å. This is indicative of only Sb–O first shell backscatters with no apparent contribution from Sb(III)–S phases. Combined with the range of energy position of peaks present in the sample first derivative XANES spectra, this suggests that the Sb_2O_3 and Sb(V) adsorbed to ferrihydrite standards are suitable Sb(III) and Sb(V) end member spectra for linear combination fitting (LCF; Fig. 1). LCF shows that there are changes in Sb speciation (Fig. 2, SI Table S2) with both sample age and depth below surface during storage. Freshly deposited tailings, the 1 year old surface sample and 3 year old subsurface samples, contain mostly reduced Sb(III) phases (58 ± 8%). Surface samples after 3 years and 8 years storage under vegetation contain progressively less Sb(III) and more Sb(V) (23 and 0% Sb(III) respectively). All the subsurface samples after 8 years storage were dominated by Sb(V) phases (2–7% Sb (III)), as was the wall drain precipitate (9% Sb(III)).

3.5. Arsenic K-edge XANES

The position of the main peak in the As K-edge XANES spectra (Fig. 3) shows that the tailings samples contain a mixture of As(III) and As(V) phases. The Fourier transformed As K-edge EXAFS data (SI Fig. S6; not phase shifted) is also consistent with a mixture of As(III)–S and As (V)–O bonding environments. LCF used FeAsS and $Ca_3(AsO_4)_2$ spectra as As(III)–S and As(V)–O end member spectra, no sample fitting required the inclusion of a contribution from the As(III)–O As_2O_3 standard spectra. The freshly deposited tailings and 1 year old surface sample were dominated by As(III)–S (94 and 93% As(III)). However, all the other samples contained predominately As(V)–O phases (34 ± 7% As (III)). The wall drain precipitate was even more As(V) dominated and contained only 7% As(III) by LCF (Fig. 3; SI Table S2).

3.6. 0.5 N HCl extractable Fe

Weak acid extractions from fresh and 1 year old tailings were dominated by Fe(II) and older samples were dominated by Fe(III) (Fig. 2). There was a noticeable increase in the total amount of extractable Fe in samples with lower Fe(II)/Fe(total) ratios (SI Table S3).

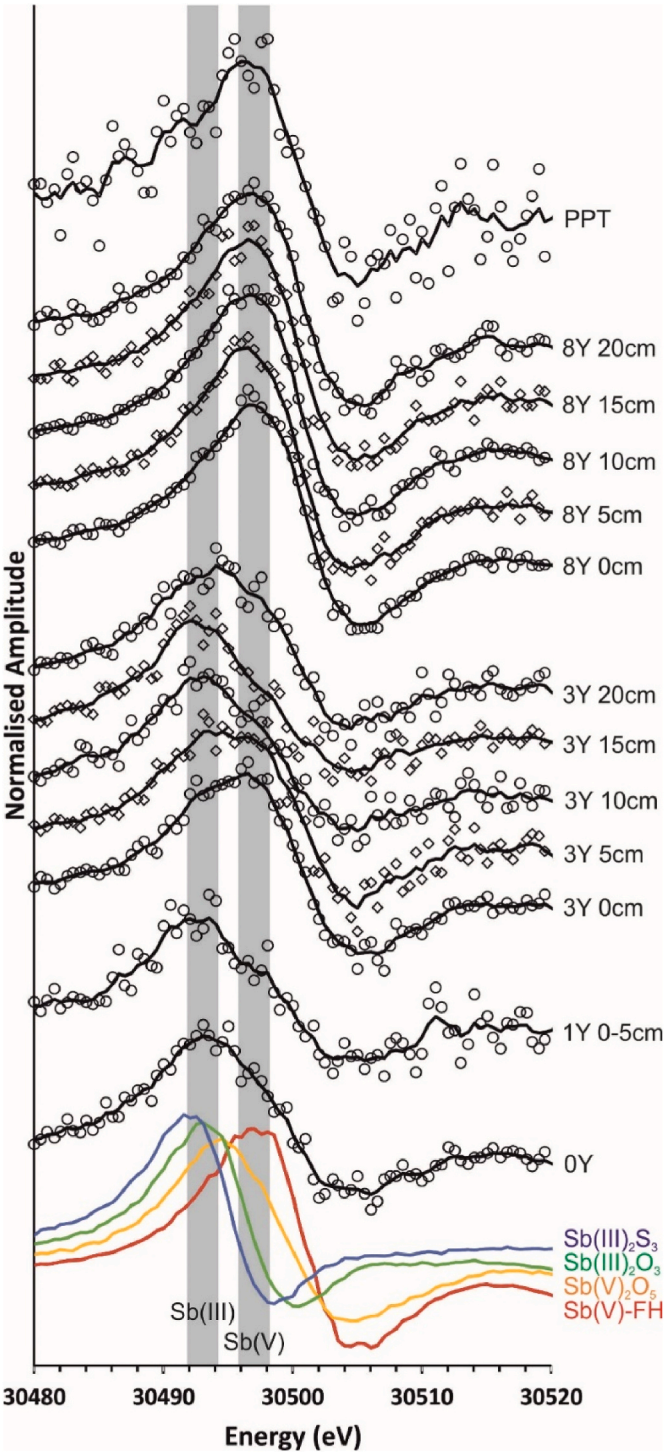

Fig. 1. Sb K-edge first derivative XANES spectra collected from tailings samples, the wall drain precipitate (PPT) and standard materials. Grey areas denote the energy position of peaks in the $Sb(III)_2O_3$ and Sb(V)-FH standard spectra. Black lines shown are weighted moving averages of sample data.

The amount of weak acid extractable Fe(II) in the tailings samples was highly correlated to Sb(III) content (Pearson's R = 0.98, p = <0.001); but there was a no significant correlation between Fe(II) and As(III) (R = 0.51, p = 0.11). Acid extractable Fe from the wall drain precipitate was dominated by Fe(III) and contained <1% extractable Fe as Fe(II).

3.7. Variation in leachable Metal(loid)s

The solution pH after 7 days mixing of deionised water (DIW) with tailings samples varied between 6.7 and 7.2 (Fig. 2, SI Table S4) with slightly higher values recorded in the older samples. Compared to bulk compositions, very low concentrations of metal(loid)s were mobilised by DIW leaching at the near neutral solution pH imposed by the tailings (SI Table S4; maximum of 2% Sb, 0.2% As, <0.1% Pb and 0.6% Zn). There were no trends in metalloid leaching with sample aging or depth, except for slightly higher Sb leaching in fresh tailings and higher Zn leaching in the 3 year old samples. In addition, no significant amounts of these metal(loid)s were mobilised from the wall drain precipitate by DIW at pH 7.5 (<0.1% of the total present was mobilised).

4. Discussion

4.1. Aging and oxidation of tailings materials under vegetation cover

Deposited Pb/Zn tailings were dominated by carbonate and silicate minerals. Sulphide minerals (such as pyrite) were present in the tailings and gypsum was present in all aged samples (and absent in fresh tailings). This provides evidence that pyrite oxidation occurs after deposition (Eqn. (1)), producing sulphate that can react with Ca^{2+} ions from calcite dissolution (Eqn. (2)) to produce gypsum (Eqn. (3)). As the tailings produce exclusively neutral leachates (Fitzsimons and Courtney, 2022), acid generation does not exceed the neutralisation capacity present.

$$2FeS_2 + 7O_2 + 2H_2O \rightarrow 2Fe^{2+} + 4SO_4^{2-} + 4H^+ \quad (1)$$

$$CaCO_3 + H^+ \rightarrow Ca^{2+} + HCO_3^{2-} \quad (2)$$

$$Ca^{2+} + SO_4^{2-} + 2H_2O \rightarrow CaSO_4{\cdot}2H_2O \quad (3)$$

This is corroborated by the changes in the ratio of Fe(II) to Fe(total) leached by weak acid solutions. The fresh tailings, the 1 year old sample and sub-surface samples from the 3 year old core were all dominated by Fe(II). However, the 3 year old surface samples contained more Fe(III), and the 8 year old core samples were Fe(III) dominated, indicating Fe(II) oxidation has occurred (Eqn. (4)). At neutral pH, $Fe^{3+}_{(aq)}$ would be expected to precipitate as iron oxyhydroxides (Eqn. (5); (Langmuir, 1997)). The accumulation of ferric oxides can also account for the observed change in sample colour over time from grey to light brown.

$$4Fe^{2+} + O_2 + 4H^+ \rightarrow 4Fe^{3+} + 2H_2O \quad (4)$$

$$Fe^{3+} + 3H_2O \rightarrow Fe(OH)_3 + 3H^+ \quad (5)$$

A sparse vegetation cover can be established in amended tailing after only 1 year but plant density is more robustly observed after 3 years. In the 3 year old core samples the effects of vegetation growth are mostly limited to a thin surface layer, with very few plant roots observed more than 5 cm below the surface, coinciding with the surface oxidation observed. In the 8 year old core samples all depths sampled have been oxidised, and the vegetation cover is well established, more diverse and with roots are found at all depths. A relationship was observed between vegetation cover and degree of oxidation, with the more oxidised tailings seemingly providing a better substrate for plant growth. This is potentially due to the reduced bioavailability of toxic elements, removal of oxygen consuming phases and introduction of new surfaces for organic C and nutrient retention (Li and Huang, 2015; Romero et al., 2007). Root growth may also help to improve soil structure in the tailings and introduce oxygen to deeper layers (Callaway and King, 1996; Cheng et al., 2022).

4.2. Effect of oxidation on As and Sb mobility

As and Sb are known to occur in Irish-type Pb/Zn ore in a range of

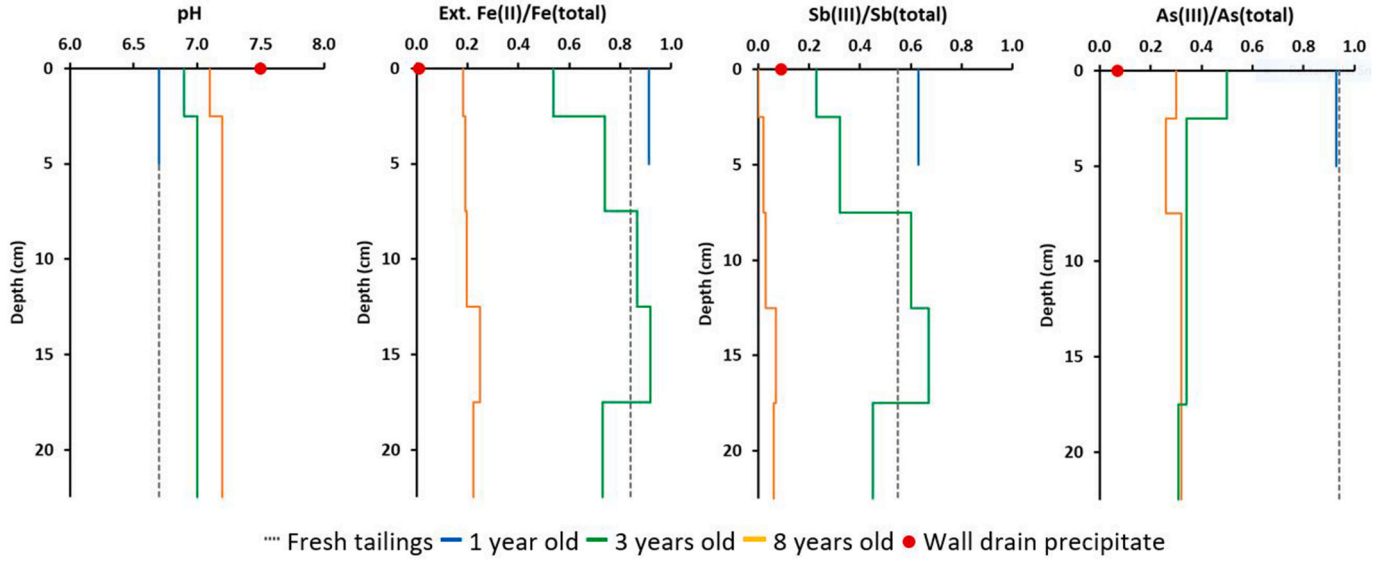

Fig. 2. Depth profiles of tailings pH, Fe(II)/Fe(total), Sb(III)/Sb(total) and As(III)/As(total).

sulphide phases including, stibnite, arsenopyrite, polymetallic Pb–Sb and Pb–As sulphide minerals (e.g. boulangerite, $Pb_5Sb_4S_{11}$; jordanite, $Pb_{14}As_6S_{23}$), and as impurities in galena, sphalerite and pyrite (Yesares et al., 2022; Wilkinson et al., 2005). Arsenic speciation in the freshly deposited and 1 year old tailings closely reflects this mineralogy with >90% of the As present in an As(III)–S bonding environment. However, the Sb k-edge EXAFS data contains only evidence for Sb–O bonds and no evidence for Sb–S bonds in any sample. Sb–S minerals such as stibnite can be rapidly oxidised in aqueous suspension, especially in the presence of pyrite, Fe^{3+} and Ca^{2+} ions which catalyse the reaction (Nan et al., 2020; Biver and Shotyk, 2012; Adelman et al., 2012). Therefore, it appears that if Sb–S species were originally present in the ore, they have been altered and partially oxidised during crushing and ore processing prior to deposition in the TMF. This is reflected in the bulk speciation of the fresh and 1 year old tailing samples, which contain an approximate 60 : 40 ratio of Sb(III)–O and Sb(V)–O phases respectively. Oxidation of Sb(III)–S is expected to produce oxyanionic species such as $Sb(III)(OH)_3$ and $Sb(V)(OH)_6^-$ (Rickard, 2012), of which the more oxidised Sb(V) species are considered more mobile in environment due to lower sorption to mineral surfaces at neutral pH (Guo et al., 2014).

In older and more surface exposed samples, both As and Sb were progressively more oxidised. Sb(III) and Fe(II) content was well correlated, indicating that both the Sb(III)–O and pyrite phases present where both oxidised at similar rates. As(III), however was not correlated Fe(II) and a portion to the As(III)–S phases present was oxidised on shorter time scales than either Sb or Fe. Significant As oxidation is observed in all the 3 year old samples, where only about 35% of the As remains in As (III)–S phases. Arsenic speciation is not appreciably changed further in the 8 year old samples, perhaps indicating that about a third of the initial As(III)–S was present in phase(s) that are less susceptible to oxidation in the tailings environment. There is no evidence for the formation of As (III)–O phases. All the oxidised As was present in the As(V)–O speciation, most likely as the arsenate oxyanion ($HAsO_4^{2-}$), which is normally considered less mobile than As(III)–O species (such as arsenite, H_3AsO_3) due to strong adsorption to minerals at neutral pH (Raven et al., 1998; Johnston et al., 2020b). In contrast to As behaviour, although some Sb (III)–O phase(s) were retained in the 3 year old samples, almost all the Sb was present as Sb(V)–O phases in the 8 year old samples.

The water leaching tests show that despite changes in bulk speciation and predicted differences in As(V) and Sb(V) mobility, the proportion of As and Sb that is leachable is very low in all samples. Therefore, although oxidation increases the proportions of As(V) and Sb(V) in the tailings, the contemporaneous formation of ferric oxides during pyrite oxidation also provides additional sorption surfaces helping to limit the mobility of both As or Sb in leachates (Mitsunobu et al., 2006).

4.3. Process occurring after emergence of tailings leachate to site drains

Despite the observed low mobility of As and Sb in the tailings, soluble As and Sb are found at μg L^{-1} concentrations in site leachates (Fitzsimons and Courtney, 2022). The leachate emerging from tailings in the upper wall drain had slightly reduced Eh and relatively high dissolved Fe(II) concentrations. Water in the wall drain flows in a thin layer over a series of cascades and sumps providing an ideal situation for aeration (Eh increases downstream from leachate sources) and ferrihydrite precipitates are found coating the surfaces of the wall drain indicating Fe(II) oxidation. Ratios of conservative indicators such dissolved sulphate and conductivity indicate that modest dilution occurs as the wall drain enters the perimeter drain. However, almost all dissolved metal(loid)s (Fe, As, Zn, Mn, Pb) had lower concentrations than would be expected by dilution alone. There is also significant accumulation of metal(loid)s (including As, Zn, Mn) within the ferrihydrite precipitates, indicating sorption of these elements to the precipitate (mostly likely including both adsorption and co-precipitation reactions). Sb does not follow this general trend and its dissolved concentrations were not reduced downstream, nor does Sb accumulate at high concentrations within the ferrihydrite precipitate (Tables 1 and 3).

At the Eh and pH values recorded in the leachates, As and Sb are predicted to be predominately present as As(V) and Sb(V) species ($HAsO_4^{2-}$ and $Sb(OH)_6^-$ respectively; (Brookins, 2012)). XANES data also indicate that only As(V)–O and Sb(V)–O phases are found in the ferrihydrite precipitate, therefore the observed difference in mobility between As and Sb in the TMF drain leachates can be ascribed to differences in the strength of bonding expected between ferrihydrite and dissolved As(V) or Sb(V) species at pH 7–8 (Guo et al., 2014; Raven et al., 1998).

4.4. Implications for tailings and leachate management

Revegetation offers benefits beyond just dust suppression and improved stability and visual appearance of the TMF. The establishment of vegetation cover is coincident with oxidation of pyrite present in the surface layers and accumulation of ferric oxides. Tailings oxidation also leads to conversion of reduced As(III)–S and Sb(III)–O phases within the

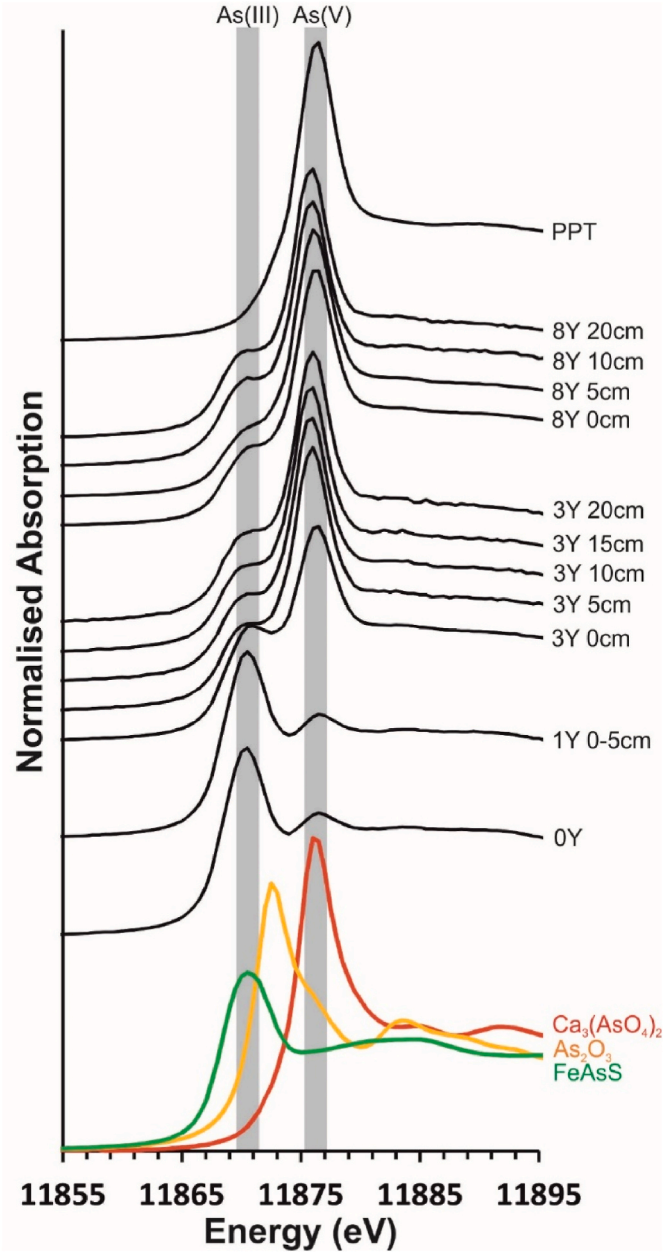

Fig. 3. As K-edge XANES spectra collected from tailings samples, the wall drain precipitate (PPT) and standard materials. Grey areas denote the energy position of peaks in the FeAs(III)S and $Ca_3(As(V)O_4)_2$ standard spectra.

tailing to oxidised As(V)–O and Sb(V)–O phases that are likely to become adsorbed to neo-formed ferric oxides and are largely immobile at neutral pH.

The leachate produced from the tailings is evidently also affected by sulphide oxidation process, and can have lower Eh (indicating oxygen depletion) and relatively high concentrations of some dissolved metal (loid)s and sulphate. However, leachates become aerated as they are collected in leachate drains. This is advantageous as it leads to Fe(II) oxidation and precipitation of ferrihydrite, which acts as a sorption surface for dissolved metal(loid)s. It may be possible to deliberately incorporate oxidation processes into future leachate management, for example by use of passive systems such as treatment wetlands or constructed aeration cascades. However, although Sb is present in tailings at relatively low solid concentrations, and is present in leachates (as $Sb(OH)_6^-$) at initially low concentrations, Sb is less effectively attenuated via sorption than other metal(loid)s present, meaning that Sb may be more problematic during leachate management. If required, removal of Sb may therefore need specifically targeted interventions, possibly including use of higher cost methods such as anion exchange resins or membrane filtration (Li et al., 2018; Long et al., 2020). This study also highlights the importance of monitoring Sb, which is often overlooked in studies of carbonate-hosted Pb and Zn mine wastes and waters (Gozzard et al., 2011; Li et al., 2022b), given its higher environmental mobility.

5. Conclusions

Vegetation cover is successfully established on Pb/Zn tailings within 3 years of seeding and application of organic compost, and is sustained and further developed after 8 years. Pyrite in the surface layers was oxidised over the same period resulting in accumulation of weak acid extractable ferric oxides. As and Sb are predominately present in freshly deposited tailings in As(III)–S and Sb(III)–O phases, but in oxidised layers As(V)–O and Sb(V)–O phases predominate. Very little As and Sb in tailings was water extractable in either freshly deposited or oxidised tailings despite changes in bulk speciation. Fe(II) containing leachate is oxidised in drainage channels leaving the TMF, resulting in a ferrihydrite precipitate that accumulated dissolved metal(loid)s, including As (V), from the leachate. Due to weak adsorption of Sb(V) species to ferrihydrite at neutral pH, Sb(V) is not accumulated in the precipitate, and further specific water treatment may be required to remove dissolved Sb prior to discharge.

Declaration of competing interest

The authors declare that they have no known competing financial interests or personal relationships that could have appeared to influence the work reported in this paper.

Data availability

Data will be made available on request.

Acknowledgements

Thanks to Oliver Fitzsimons (Environmental Department, Boliden Tara Mines, Ireland) for access to the Tara Mines TMF and guidance during sampling. Special thanks to Scott Johnston (Southern Cross University, Australia) for sharing XAS data for Sb absorbed to ferrihydrite standard. We acknowledge support from Engineering and Physical Science Research Council grant EP/T031166/1, Diamond Light Source for time on Beamline B18 under Proposal SP29970 and help from beamline scientist, Nitya Ramanan. Lesley Neve, Fiona Keay and Stephen Reid are also acknowledged for help in XRD, XRF, IC and ICP-OES/MS analysis.

Appendix A. Supplementary data

Supplementary data to this article can be found online at https://doi.org/10.1016/j.apgeochem.2023.105806.

References

Adelman, J., Beauchemin, S., Hendershot, W., Kwong, Y., 2012. Change in the Oxidation Rate of Stibnite as Affected by Pyrite in an Oxygenated Flow-Through System.

Bennett, W.W., Hockmann, K., Johnston, S.G., Burton, E.D., 2017. Synchrotron X-ray absorption spectroscopy reveals antimony sequestration by reduced sulfur in a freshwater wetland sediment. Environ. Chem. 14, 345–349.

Biver, M., Shotyk, W., 2012. Stibnite (Sb2S3) oxidative dissolution kinetics from pH 1 to 11. Geochem. Cosmochim. Acta 79, 127–139.

Bray, A.W., Stewart, D.I., Courtney, R., Rout, S.P., Humphreys, P.N., Mayes, W.M., Burke, I.T., 2018. Sustained bauxite residue rehabilitation with gypsum and organic matter 16 years after initial treatment. Environ. Sci. Technol. 52, 152–161.

Brookins, D.G., 2012. Eh-pH Diagrams for Geochemistry. Springer Science & Business Media.

Callaway, R.M., King, L., 1996. Temperature-driven variation in substrate oxygenation and the balance of competition and facilitation. Ecology 77, 1189–1195.
Chambers, J.C., Sidle, R.C., 1991. Fate of Heavy Metals in an Abandoned Lead-Zinc Tailings Pond: I. Vegetation. Wiley Online Library.
Cheng, Y., Bu, X., Li, J., Ji, Z., Wang, C., Xiao, X., Li, F., Wu, Z.-H., Wu, G., Jia, P., 2022. Application of biochar and compost improved soil properties and enhanced plant growth in a Pb–Zn mine tailings soil. Environ. Sci. Pollut. Control Ser. 1–11.
Filella, M., Belzile, N., Chen, Y.-W., 2002. Antimony in the environment: a review focused on natural waters: I. Occurrence. Earth Sci. Rev. 57, 125–176.
Fitzsimons, O., Courtney, R., 2022. Characterisation of Pb/Zn tailings and drainage waters to inform post-closure water treatment strategies. Mine Water Environ.
Gozzard, E., Mayes, W.M., Potter, H.A.B., Jarvis, A.P., 2011. Seasonal and spatial variation of diffuse (non-point) source zinc pollution in a historically metal mined river catchment, UK. Environ. Pollut. 159, 3113–3122.
Guilbert, J.M., Park Jr., C.F., 2007. The Geology of Ore Deposits. Waveland Press.
Guo, X., Wu, Z., He, M., Meng, X., Jin, X., Qiu, N., Zhang, J., 2014. Adsorption of antimony onto iron oxyhydroxides: adsorption behavior and surface structure. J. Hazard Mater. 276, 339–345.
Heikkinen, P., Räisänen, M., Johnson, R., 2009. Geochemical characterisation of seepage and drainage water quality from two sulphide mine tailings impoundments: acid mine drainage versus neutral mine drainage. Mine Water Environ. 28, 30–49.
Hudson-Edwards, K.A., Byrne, P., Bird, G., Brewer, P.A., Burke, I.T., Jamieson, H.E., Macklin, M.G., Williams, R.D., 2019. Origin and Fate of vanadium in the hazeltine creek catchment following the 2014 Mount Polley Mine tailings spill in British Columbia, Canada. Environ. Sci. Technol. 53, 4088–4098.
Hudson-Edwards, K.A., Macklin, M.G., Jamieson, H.E., Brewer, P.A., Coulthard, T.J., Howard, A.J., Turner, J.N., 2003. The impact of tailings dam spills and clean-up operations on sediment and water quality in river systems: the Ríos Agrio–Guadiamar, Aznalcóllar, Spain. Appl. Geochem. 18, 221–239.
Janković, S., Mozgova, N., Borodaev, Y.S., 1977. The complex antimony-lead/zinc deposit at Rujevac/Yugoslavia; its specific geochemical and mineralogical features. Miner. Deposita 12, 381–392.
Johnston, S.G., Bennett, W.W., Doriean, N., Hockmann, K., Karimian, N., Burton, E.D., 2020a. Antimony and arsenic speciation, redox-cycling and contrasting mobility in a mining-impacted river system. Sci. Total Environ. 710, 136354.
Johnston, S.G., Karimian, N., Burton, E.D., 2020b. Seasonal temperature oscillations drive contrasting arsenic and antimony mobilization in a mining-impacted river system. Water Resour. Res. 56, e2020WR028196.
Jones, A., Rogerson, M., Greenway, G., Potter, H., Mayes, W., 2013. Mine water geochemistry and metal flux in a major historic Pb-Zn-F orefield, the Yorkshire Pennines, UK. Environ. Sci. Pollut. Control Ser. 20, 7570–7581.
Jordan, S.N., Mullen, G.J., Courtney, R.G., 2008. Utilization of spent mushroom compost for the revegetation of lead–zinc tailings: effects on physico-chemical properties of tailings and growth of Lolium perenne. Bioresour. Technol. 99, 8125–8129.
Kossoff, D., Dubbin, W., Alfredsson, M., Edwards, S., Macklin, M., Hudson-Edwards, K.A., 2014. Mine tailings dams: characteristics, failure, environmental impacts, and remediation. Appl. Geochem. 51, 229–245.
Langmuir, D., 1997. Aqueous Environmental. Geochemistry Prentice Hall, Upper Saddle River, NJ, 600.
Li, J., Zheng, B., He, Y., Zhou, Y., Chen, X., Ruan, S., Yang, Y., Dai, C., Tang, L., 2018. Antimony contamination, consequences and removal techniques: a review. Ecotoxicol. Environ. Saf. 156, 125–134.
Li, X., Huang, L., 2015. Toward a new paradigm for tailings phytostabilization—nature of the substrates, amendment options, and anthropogenic pedogenesis. Crit. Rev. Environ. Sci. Technol. 45, 813–839.
Li, X., Zhou, T., Li, Z., Wang, W., Zhou, J., Hu, P., Luo, Y., Christie, P., Wu, L., 2022a. Legacy of contamination with metal (loid) s and their potential mobilization in soils at a carbonate-hosted lead-zinc mine area. Chemosphere 308, 136589.
Li, X., Zhou, T., Li, Z., Wang, W., Zhou, J., Hu, P., Luo, Y., Christie, P., Wu, L., 2022b. Legacy of contamination with metal(loid)s and their potential mobilization in soils at a carbonate-hosted lead-zinc mine area. Chemosphere 308, 136589.
Long, X., Wang, X., Guo, X., He, M., 2020. A review of removal technology for antimony in aqueous solution. J. Environ. Sci. 90, 189–204.
Lovley, D.R., Phillips, E.J.P., 1986. Availability of ferric iron for microbial reduction in bottom sediments of the freshwater tidal potomac river. Appl. Environ. Microbiol. 52, 751–757.
Mcgrory, E.R., Brown, C., Bargary, N., Williams, N.H., Mannix, A., Zhang, C., Henry, T., Daly, E., Nicholas, S., Petrunic, B.M., 2017. Arsenic contamination of drinking water in Ireland: a spatial analysis of occurrence and potential risk. Sci. Total Environ. 579, 1863–1875.
Mitsunobu, S., Harada, T., Takahashi, Y., 2006. Comparison of antimony behavior with that of arsenic under various soil redox conditions. Environ. Sci. Technol. 40, 7270–7276.
Mudd, G., Boger, D., 2013. The ever growing case for paste and thickened tailings—towards more sustainable mine waste management. J. Aust. Inst. Min. Metall 2, 56–59.
Nan, J., Xiaoqian, L., Aiguo, Z., Yuliu, H., Guofang, P., 2020. Effect of pH value and Fe (III) on the oxidative dissolution of stibnite. 地质科技通报 39, 76–84.
Olszewska, J.P., Meharg, A.A., Heal, K.V., Carey, M., Gunn, I.D., Searle, K.R., Winfield, I. J., Spears, B.M., 2016. Assessing the legacy of red mud pollution in a shallow freshwater lake: arsenic accumulation and speciation in macrophytes. Environ. Sci. Technol. 50, 9044–9052.
Othmani, M.A., Souissi, F., Benzaazoua, M., Bouzahzah, H., Bussiere, B., Mansouri, A., 2013. The geochemical behaviour of mine tailings from the Touiref Pb-Zn District in Tunisia in weathering cells leaching tests. Mine Water Environ. 32, 28.
Plante, B., Benzaazoua, M., Bussière, B., 2011. Predicting geochemical behaviour of waste rock with low acid generating potential using laboratory kinetic tests. Mine Water Environ. 30, 2–21.
Proto, M., Newsome, L., Jensen, E., Courtney, R., 2022. Geochemical analyses of metal (loid) fractions do not predict plant uptake behavior: are plant bioassays better tools to predict mine rehabilitation success? Sci. Total Environ., 160679
Ravel, B., Newville, M., 2005. Athena, artemis, hephaestus: data analysis for X-ray absorption spectroscopy using IFEFFIT. J. Synchrotron Radiat. 12, 537–541.
Raven, K.P., Jain, A., Loeppert, R.H., 1998. Arsenite and arsenate adsorption on ferrihydrite: kinetics, equilibrium, and adsorption envelopes. Environ. Sci. Technol. 32, 344–349.
Rickard, D., 2012. Chapter 4 - aqueous metal–sulfide chemistry: complexes, clusters and nanoparticles. In: Rickard, D. (Ed.), Developments in Sedimentology. Elsevier.
Romero, F., Armienta, M., González-Hernández, G., 2007. Solid-phase control on the mobility of potentially toxic elements in an abandoned lead/zinc mine tailings impoundment, Taxco, Mexico. Appl. Geochem. 22, 109–127.
Su, Z., Chen, Q., Zhang, Q., Zhang, D., 2019. Recycling lead–zinc tailings for cemented paste backfill and stabilisation of excessive metal. Minerals 9, 710.
Warnken, J., Ohlsson, R., Welsh, D.T., Teasdale, P.R., Chelsky, A., Bennett, W.W., 2017. Antimony and arsenic exhibit contrasting spatial distributions in the sediment and vegetation of a contaminated wetland. Chemosphere 180, 388–395.
Wilkinson, J., Eyre, S., Boyce, A., 2005. Ore-forming processes in Irish-type carbonate-hosted Zn-Pb deposits: evidence from mineralogy, chemistry, and isotopic composition of sulfides at the Lisheen mine. Econ. Geol. 100, 63–86.
Yesares, L., Menuge, J.F., Blakeman, R.J., Ashton, J.H., Boyce, A.J., Coller, D., Drummond, D.A., Farrelly, I., 2022. Pyritic mineralization halo above the Tara Deep Zn-Pb deposit, Navan, Ireland: evidence for sub-seafloor exhalative hydrothermal processes? Ore Geol. Rev. 140, 104415.